ENVIRONMENTAL STUDIES

Widespread formation of toxic nitrated bisphenols indoors by heterogeneous reactions with HONO

Diwen Yang[1], Qifan Liu[1,2], Sizhi Wang[1], Matin Bozorg[1], Jiabao Liu[1,3], Pranav Nair[1], Patrick Balaguer[4], Datong Song[1], Henry Krause[3], Boualem Ouazia[5], Jonathan P. D. Abbatt[1], Hui Peng[1,6]*

With numerous structurally diverse indoor contaminants, indoor transformation chemistry has been largely unexplored. Here, by integrating protein affinity purification and nontargeted mass spectrometry analysis (PUCA), we identified a substantial class of previously unrecognized indoor transformation products formed through gas-surface reactions with nitrous acid (HONO). Through the PUCA, we identified a noncommercial compound, nitrated bisphenol A (BPA), from house dust extracts strongly binding to estrogen-related receptor γ. The compound was detected in 28 of 31 house dust samples with comparable concentrations (ND to 0.30 μg/g) to BPA. Via exposing gaseous HONO to surface-bound BPA, we demonstrated it likely forms via a heterogeneous indoor chemical transformation that is highly selective toward bisphenols with electron-rich aromatic rings. We used ^{15}N-nitrite for in situ labeling and found 110 nitration products formed from indoor contaminants with distinct aromatic moieties. This study demonstrates a previously unidentified class of chemical reactions involving indoor HONO, which should be incorporated into the risk evaluation of indoor contaminants, particularly bisphenols.

INTRODUCTION

Humans spend about 90% of their lives indoors, where they are exposed to most of their chemical exposure from a "cocktail" of numerous synthetic chemicals (*1*, *2*). A large fraction of these chemicals originates from the volatilization, abrasion, and leaching of commercial products (*3*). Some of these contaminants can exert toxic effects by entering human bodies via air inhalation, dermal exposure, or dust ingestion (*3*). For example, bisphenols, including bisphenol A (BPA), a significant class of endocrine-disrupting chemicals widely detected in indoor environments, have been associated with a range of adverse health effects, including disorders of the reproductive, neuroendocrine, and immune systems (*4*–*6*). It is essential to investigate the source, presence, and environmental fate of indoor contaminants.

In response to potential human exposure risks, substantial effort has been invested in determining the concentrations of commercial chemicals in the indoor environment (e.g., in the air, in dust, and on surfaces) and their toxicological effects (*7*–*11*). However, it has recently been recognized that commercial chemicals may undergo reactions with oxidants, such as ozone (O_3), once released into the indoor environment (*12*–*16*). The transformation products are of great concern given their potentially higher toxicities than those of their precursor compounds, as exemplified by the formation of carcinogenic carbonyls from unsaturated lipids through reactions with O_3 (*17*–*20*). Also, nicotine from tobacco smoke adsorbed onto indoor surfaces is converted to carcinogenic nitrosamines via a heterogeneous reaction with indoor gaseous nitrous acid (HONO) (*21*). Although very high mixing ratios [up to 14 parts per billion (ppb)] of HONO have been detected inside (*22*, *23*), little is known about the gas-surface heterogeneous reactions in which it participates. Together, these results underscore the need to consider chemical transformations when assessing the health risks arising from indoor synthetic chemicals.

The reaction products of many synthetic chemicals used indoors and their associated health impacts are largely unknown (*13*, *16*). This is because of the limited capacity of conventional toxicity testing strategies on individual chemicals (*24*). Given the immense number (>350,000) of synthetic chemicals and their diverse structures (*25*), the indoor transformations of these species are extremely complex, and authentic standards for most transformation products are not available. Moreover, the toxicity of the transformation products can be completely different from that of their precursor chemicals, even with minor structural changes (*26*–*28*). These two factors make the identification of indoor transformation products and elucidation of their toxicity very challenging with conventional approaches. To address this issue, we have proposed a new "top-down" strategy that uses protein-guided purification in combination with high-resolution mass spectrometry (HRMS)–based untargeted analysis (PUCA) to directly identify potentially toxic chemicals from environmental chemical cocktails (*29*–*31*). With this method, both known and unknown chemicals (including their transformation products) binding to the key proteins of interest can be isolated and identified in an unbiased manner (Fig. 1A).

Here, using the PUCA approach, we found a previously unrecognized toxic nitrated BPA (NO_2-BPA) in indoor dust. NO_2-BPA binds strongly to the human estrogen-related receptor γ (ERRγ), which is an essential regulator protein in multiple endocrine and metabolic pathways and associated diseases (*32*), such as insulin resistance (*33*) and alcoholic liver injury (*34*). Using laboratory experiments, we demonstrated that NO_2-BPA is likely formed through the heterogeneous dark reaction between gas-phase indoor HONO and surface-bound BPA. Beyond NO_2-BPA, 110 additional nitrated contaminants with distinct aromatic moieties were detected in indoor dust. This points to the HONO-BPA chemistry described here as just one specific example of a previously unrecognized and widespread class of transformation reactions involving numerous indoor

[1]Department of Chemistry, University of Toronto, Toronto, ON, Canada. [2]Department of Environmental Science and Engineering, University of Science and Technology of China, Hefei, China. [3]The Donnelly Centre, University of Toronto, Toronto, ON, Canada. [4]IRCM, INSERM U1194, Université de Montpellier, ICM, Montpellier, France. [5]National Research Council Canada, Ottawa, ON, Canada. [6]School of the Environment, University of Toronto, Toronto, ON, Canada.
*Corresponding author. Email: hui.peng@utoronto.ca

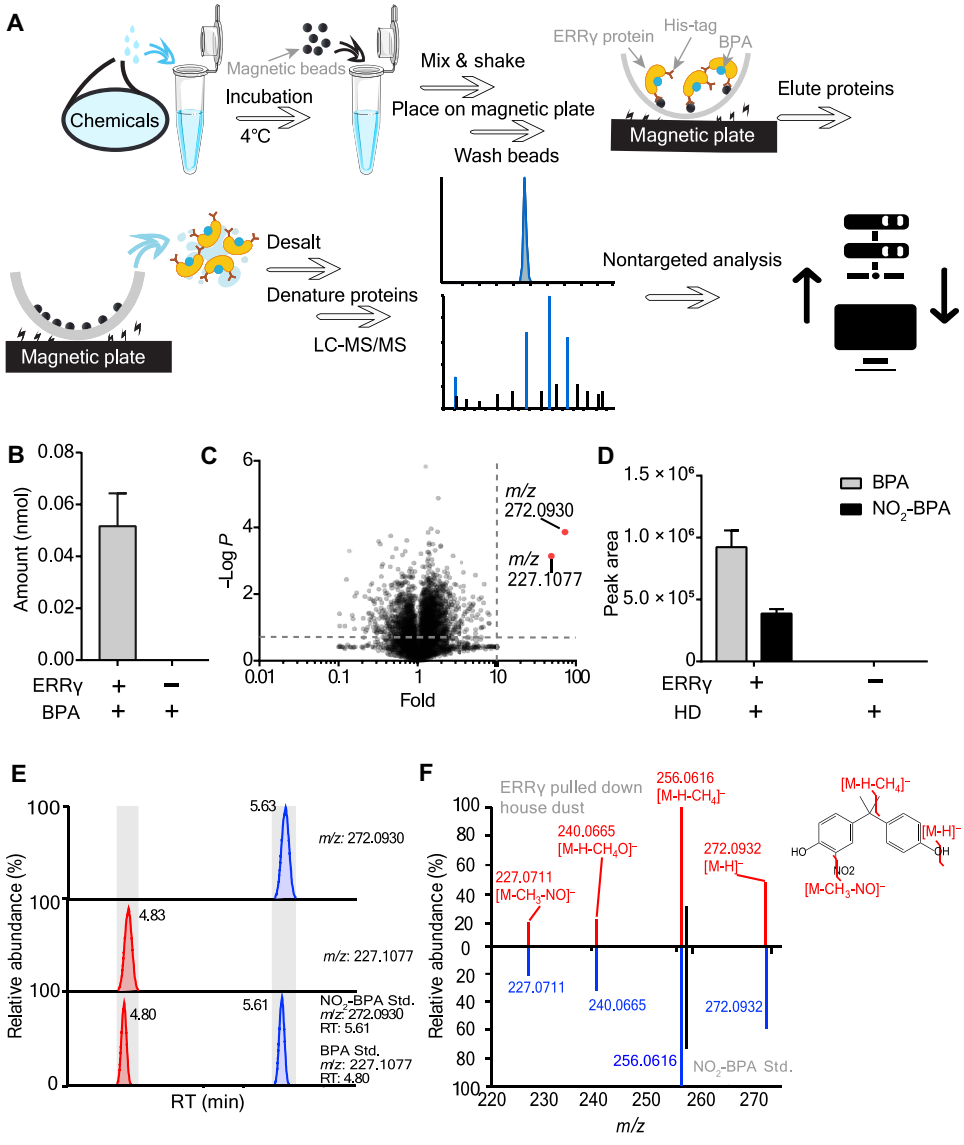

Fig. 1. Identification of NO_2-BPA as a previously unknown contaminant binding to estrogen-related receptor γ. (**A**) The workflow of the PUCA method used to identify unknown ligands binding to estrogen-related receptor γ (ERRγ). LC-MS/MS, liquid chromatography–tandem mass spectrometry. (**B**) Benchmarking the PUCA method using BPA as the positive control. The addition (+) and absence (−) of the ingredients in the reactions are shown beneath the figure. (**C**) Volcano plot representing the log-transformed ratios and corresponding *P* values of LC-MS peak features. The horizontal gray line indicates the cutoff of fold change (fold > 10). The vertical line shows the cutoff of the log *P* value (−log*P* > 1.30). The red dots show the peak features that fulfilled the cutoffs. (**D**) The peak area of BPA and unknown (NO_2-BPA) compound pulled out by ERRγ compared to the absence of the protein (negative control) when exposed to house dust (HD) extracts. (**E**) The retention time (RT) of BPA and unknown (NO_2-BPA) on a C18 column. The chromatograms of BPA and NO_2-BPA in dust are shown in the top and middle, while their standard mixture is shown in the bottom. (**F**) The MS^2 spectrum of the unknown compound in dust extract (red) compared to the spectrum of synthesized NO_2-BPA (blue). Data are presented from one representative experiment of three experiments performed with similar results.

aromatic contaminants. These results highlight the need to include this newly found HONO chemistry in the risk evaluation of indoor contaminants, particularly for bisphenols.

RESULTS

Protein-guided identification of nitrated BPA as a new indoor contaminant

To identify the toxic contaminants binding to ERRγ from indoor dust, we overexpressed the His-tagged ligand-binding domain (LBD) of human ERRγ in *Escherichia coli* (fig. S1) to isolate ligands using the PUCA platform. For the proof of concept, the platform was first benchmarked with BPA, a well-known agonist of ERRγ with a nanomolar affinity (*35*). After incubating environmentally relevant concentrations (0.1 nmol in 400 μl) of BPA with ERRγ overexpressed in *E. coli* lysate, the complex of BPA and His-tagged ERRγ was isolated by magnetic nickel beads. The complexes were further subjected to nondenaturing size exclusion chromatography to remove nonspecific binding interferences (Fig. 1A). BPA (0.052 ± 0.010 nmol) was pulled out by the ERRγ LBD but not by the wild-type *E. coli* lysates (Fig. 1B).

The results demonstrated that the PUCA platform can selectively pull out the ligands binding to ERRγ with a good recovery efficiency.

We then applied the PUCA platform to directly identify previously unknown ERRγ ligands from the extracts of indoor dust samples that contain thousands of co-occurring compounds. While 12,608 liquid chromatography–mass spectrometry (LC-MS) peak features were detected in the pulldown extracts as indoor chemicals and background contaminants from the extraction solvent and liquid chromatography mobile phase, only 2 LC-MS peak features were selectively pulled out by the *E. coli* lysates overexpressing ERRγ, with 73- and 48-fold higher abundances than the wild-type *E. coli* lysates (negative control) ($P < 0.001$; Fig. 1, C and D). The LC-MS peak feature with a mass/charge ratio (m/z) of 227.1077 was confirmed as BPA ($[M\text{-}H]^-$) by its authentic standard (Fig. 1E). This is not unexpected as BPA is a well-documented contaminant that has been frequently detected indoors (*4*, *7*, *8*). The results confirm the validity of using the PUCA platform to effectively pull out ERRγ ligands from the complex chemical mixtures within house dust. The higher–molecular weight species at m/z = 272.0930 was detected at a longer retention time (5.63 min) than BPA (4.83 min) on a C18 column, reflecting its higher hydrophobicity. The chemical formula of this feature corresponds to $[C_{15}H_{14}NO_4]^-$ with a mass error of 0.62 parts per million (ppm). None of the formulae of the chemicals within the Toxic Substances Control Act (TSCA) database (which contains all the produced chemicals in the United States without qualifying for an exemption or exclusion under TSCA) match the predicted formula (*36*). This demonstrates that the chemical at m/z = 272.0930 is a previously unrecognized contaminant without inventory records within the available database.

To identify the structure of this contaminant, we further analyzed its high-resolution MS^2 spectrum. Among several predominant MS^2 fragments, BPA at m/z 227.0713 was detected with high abundance (Fig. 1F) with a neutral loss of NO ($[M\text{-}CH_3\text{-}NO]^-$), indicating that this contaminant is a potential BPA derivative. Given that the neutral loss of NO is a characteristic fragmentation pathway for nitroaromatic compounds (*9*, *37*), this contaminant is assigned as nitrated BPA (NO_2-BPA), with the structure shown in Fig. 1F. To confirm the identity of NO_2-BPA, we synthesized this compound in the laboratory, with the nuclear magnetic resonance (NMR) spectrum provided in fig. S2. As shown in Fig. 1F, the MS^2 spectrum and retention time of the synthesized NO_2-BPA exactly match the peak feature from the pulldown extract, confirming the identification of $[C_{15}H_{14}NO_4]^-$.

Validation of NO_2-BPA as a high-affinity ERRγ ligand

To verify that NO_2-BPA is an ERRγ ligand, we used the isothermal titration calorimetry (ITC) approach to determine the binding affinity between the synthesized NO_2-BPA and purified ERRγ LBD. A strong interaction was detected between NO_2-BPA and ERRγ with a dissociation constant (K_D) of 0.36 μM (Fig. 2A). This strong interaction is also indicated by the measured thermal stability for ERRγ LBD, which showed that the melting temperature of ERRγ LBD increased from 45° to 55°C with the presence of 25 μM NO_2-BPA (Fig. 2B). This demonstrates that the binding of NO_2-BPA strengthens the thermal stability of ERRγ LBD.

We also used the Lanthanide Chelate Excite-time resolved fluorescence resonance energy transfer (LANCE-FRET) assay to test whether the binding of NO_2-BPA to ERRγ LBD facilitates the recruitment of cofactors. With the presence of NO_2-BPA, Peroxisome proliferator-activated receptor-gamma coactivator (PGC)-1α was significantly recruited to ERRγ LBD, as reflected by the increase in fluorescence at 520 nm (Fig. 2C). The median effective concentration of NO_2-BPA to induce PGC1α was determined as 0.40 μM, comparable to the result of ITC. Then, we used the human cells transfected with ERRγ to assess the impact of NO_2-BPA on the transcriptional activity of ERRγ (Fig. 2D). As ERRγ is constitutively activated in the absence of ligand, 0.3 μM 4-hydroxytamoxifen (4OH-TAM) was used to inhibit the baseline activity as the control. Compared to the control, a dose-dependent induction of luciferase was observed, as shown in Fig. 2D, with a concentration above 0.3 μM. This confirms that NO_2-BPA is a high-affinity agonist for ERRγ. To better understand the binding site of NO_2-BPA to ERRγ, we performed a molecular docking analysis. The free energy (ΔG) of the interaction was calculated to be −8.98 kcal/mol by AutoDock4. The binding pose of NO_2-BPA is similar to that of BPA cocrystallized with ERRγ, with an additional hydrogen bond formed between Arg^{316} and the nitro group (Fig. 2E). The importance of the hydrogen bond is also consistent with the aforementioned ITC results, which show that the enthalpy of binding ($-\Delta H$, 18.4 kcal/mol) is double the entropic term (TΔS, 9.7 kcal/mol; Fig. 2A).

Widespread indoor contaminant NO_2-BPA formed through reaction with HONO

Among the 31 house dust samples, NO_2-BPA was detected in 28 samples with a detection frequency of 90.3%, indicating its nearly ubiquitous presence in the indoor environment. The concentrations of NO_2-BPA ranged from below the detection limit (ND) to very high levels of 0.30 μg/g, i.e., comparable to those of the well-known contaminant BPA (ND to 5.29 μg/g; Fig. 3, A and B). As mentioned earlier, NO_2-BPA is not included in the TSCA database, i.e., it is unlikely to have a direct emission source. Given this, one explanation for the presence of this contaminant is that it is formed through indirect indoor chemical transformation. HONO is present in indoor residential environments at high mixing ratios (*22*, *23*), and it can nitrate 3-methylcatechol (*38*); we decided to focus on heterogeneous nitration of BPA by HONO. In particular, because of its low volatility (*39*), BPA will be largely present in particles or on surfaces indoors; also, it has been deduced that HONO exists in large amounts as nitrite on indoor surfaces (*22*, *40*). While it is possible that other nitrating mechanisms exist, such as heterogeneous reaction with NO_3, the heterogeneous reactivity of NO_3 with phenolic substances is not known, and NO_3 mixing ratios indoors are not well characterized.

To confirm this "HONO transformation hypothesis," we performed heterogeneous HONO reactivity experiments with BPA coated on glass slides (estimated average coating thickness of ~1 nm). Significant formation of NO_2-BPA [product-to-parent ratio ($R_{product}$) = 0.04 ± 0.006%] was observed after reaction with 15 ppb of gaseous HONO for 12 hours (Fig. 3C), significantly higher than that detected in the control experiments in the absence of HONO. This demonstrated that NO_2-BPA can be formed through gas-surface heterogeneous HONO chemistry. Note that the reaction time used in this study is much shorter than the dust residence time in actual indoor environments where the NO_2-BPA ratio is high.

In addition to BPA, many other bisphenols, such as bisphenol B (BPB; structure is shown in Fig. 3D) and bisphenol S (BPS; 4,4′-sulfonyldiphenol), have also been widely detected in the indoor environment (*8*). Motivated by the discovery of NO_2-BPA, we further

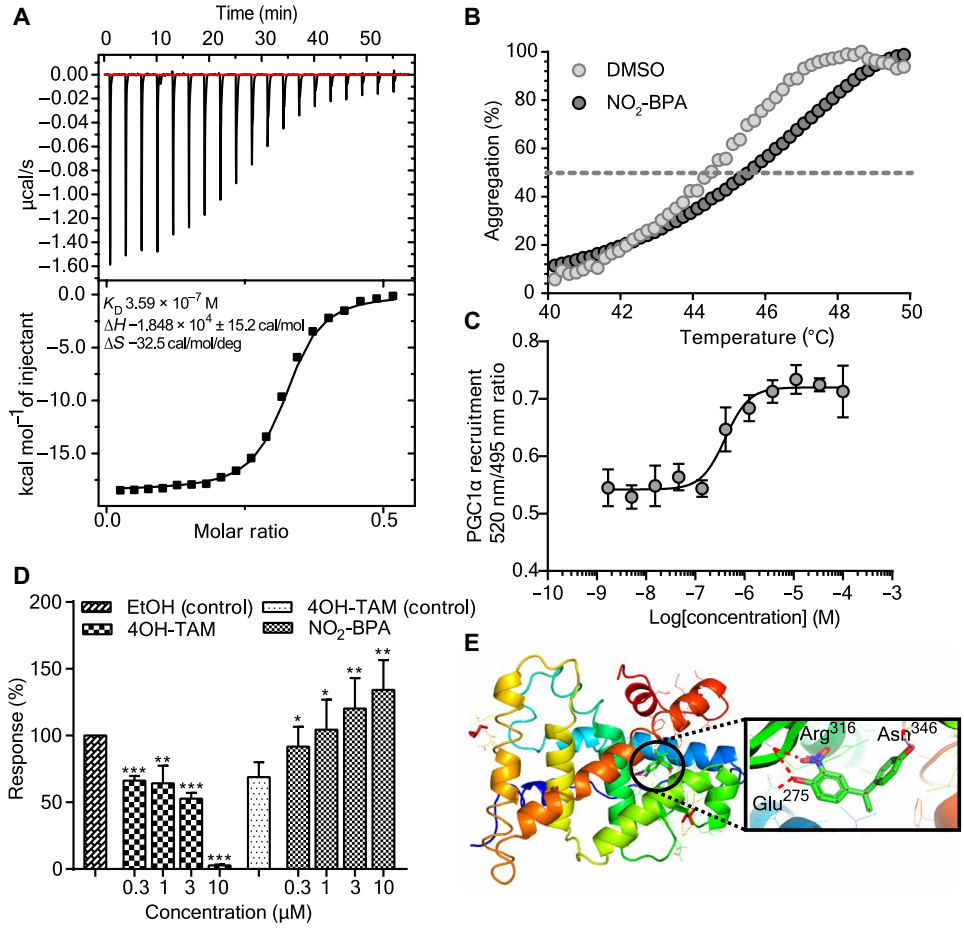

Fig. 2. NO_2-BPA binds to ERRγ with a high binding affinity. (**A**) ITC thermogram (top) and the corresponding measured K_D, entropy (ΔS), and enthalpy (ΔH) of NO_2-BPA binding to ERRγ LBD according to the molar ratio (bottom). (**B**) Thermal shift assays demonstrated the strong physical interaction between NO_2-BPA and ERRγ LBD. DMSO, dimethyl sulfoxide. (**C**) The bioactivation of ERRγ by NO_2-BPA is shown via recruiting a cofactor, PGC1α, in LANCE nuclear receptor assay. (**D**) The luciferase activity of HG5LN-ERRγ cells when exposed to NO_2-BPA and its known antagonist, 4OH-TAM. $^*P < 0.05$, $^{**}P < 0.01$, and $^{***}P < 0.001$. EtOH, ethanol. (**E**) The molecular docking result of NO_2-BPA binding to ERRγ with three hydrogen bonds (Glu^{275}, Asn^{346}, and Arg^{316}). Data are presented from one representative experiment of two experiments performed with similar results.

investigated the occurrence of nitrated BPB and BPS analogs by searching the indoor dust extracts for their predicted LC-MS peaks within a mass tolerance of 2 ppm. Supporting our hypothesis, nitrated BPB (NO_2-BPB) was also detected in house dust with a shorter retention time (7.01 min) than BPB (7.72 min; Fig. 3D). The identity of NO_2-BPB was confirmed by detecting NO neutral loss in MS^2 spectra. While BPS was detected with an even higher abundance than BPA in house dust, its nitrated analog was not detected. This demonstrated that HONO might selectively react with BPA and BPB but not BPS. To confirm this, we performed the heterogeneous reaction between gaseous HONO and BPB and BPS films using the same experimental conditions for BPA. Consistent with the house dust results, NO_2-BPB ($R_{product}$ = 0.2 ± 0.28%) was formed at significant levels through reaction with HONO, but nitrated BPS (NO_2-BPS) was not detected (Fig. 3C).

Motivated by the high selectivity of heterogeneous HONO reactions, we further investigated the structure-related reactivity of HONO with eight commonly detected indoor phenolic contaminants (see structures in Fig. 4A) in aqueous solutions, where a high concentration of nitrite (leading to high concentrations of HONO, with sufficient acidity: $H^+ + NO_2^- \rightarrow HONO$) can be used to accelerate the reaction. Consistent with the heterogeneous reactivity results, selective formation was observed for NO_2-BPA and NO_2-BPB but not for NO_2-BPS after reaction with 10 mM nitrite for 24 hours in the dark (Fig. 4B). Among the eight investigated phenols, 4,4′-thiobis(2-tert-butyl-5-methylphenol) (AO44S25) is the most reactive compound, but its $R_{product}$ at 8 hours decreased because of the formation of the dinitrated product. High reactivity toward HONO was also observed for bisphenol F (BPF; 4,4′-methylenediphenol; Fig. 4B), another bisphenol analog widely detected in house dust (*8*), with a $R_{product}$ of 2193 ± 86% after 24 hours of reaction. Similar to BPS, the nitration product was not observed for bisphenol AF (BPAF), likely because of the electron-withdrawing effect of fluorine. As nucleophilicity is typically related to the energy of the highest occupied molecular orbital (HOMO), we calculated the HOMO for all eight compounds. A clear decrease in $R_{product}$ was observed along with lower HOMO energy, especially for the single-ring phenols [4-nonylphenol (4-NP) and 4-tertoctylphenol (4-OP)], which showed two orders of magnitude lower $R_{product}$ than bisphenols (Fig. 4C). Collectively, these results demonstrate that HONO, acting

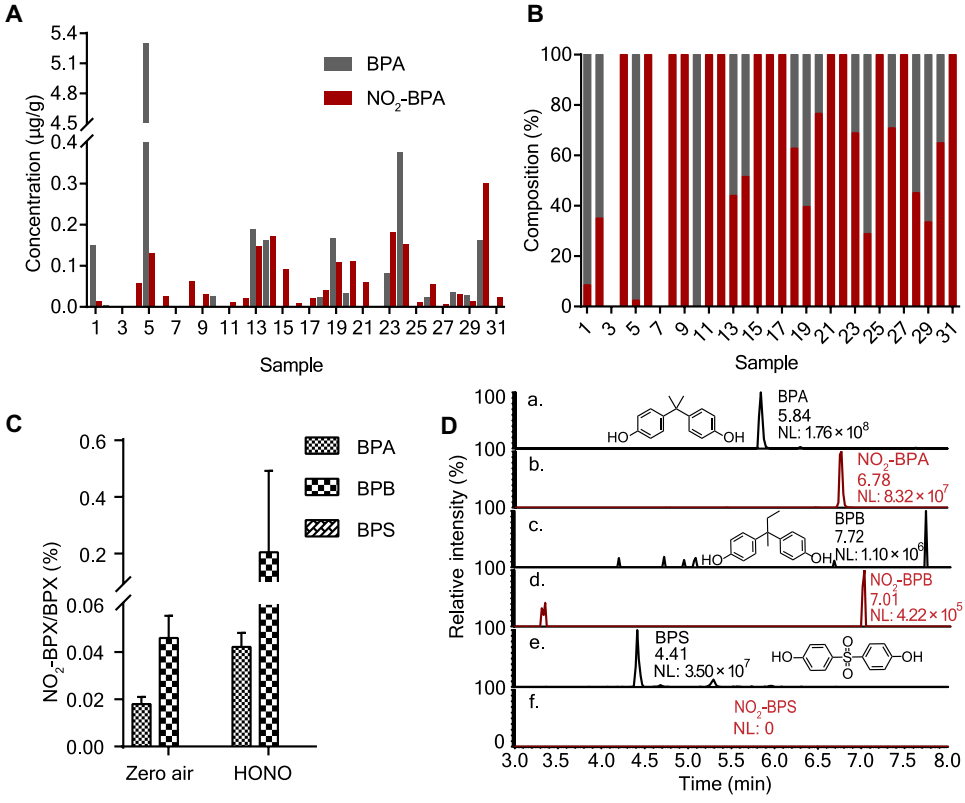

Fig. 3. Occurrence and formation of NO_2-BPA and bisphenol analogs. (**A**) The concentrations of NO_2-BPA and BPA in 31 house dust samples. (**B**) The relative compositions of NO_2-BPA and BPA in the 31 house dust samples. (**C**) The ratio of NO_2-BPA, NO_2-BPB, and NO_2-BPS to the corresponding native compounds (BPA, BPB, and BPS) after heterogeneous HONO reactions. A negligible amount of NO_2-BPA was also detected from the control in the absence of HONO, which may be formed through reaction with ambient HONO during the extraction and instrumental analysis procedure. NO_2-BPS was not shown in the figure as it was not detected. Data are presented from one representative experiment of two experiments performed with similar results. (**D**) The HPLC chromatograms indicate the detection of NO_2-BPA and NO_2-BPB in house dust samples but not NO_2-BPS. Three bisphenol analogs (BPA, BPB, and BPS) are shown in **a**, **c**, and **e**, and NO_2-BPA and NO_2-BPB are shown in **b** and **d**, respectively. NO_2-BPS was not detected, as shown in **f**. NL, normalization level.

as an electrophile, selectively reacts with bisphenols with stronger nucleophilicity or higher HOMO energy.

To better understand the impacts of environmental conditions on the reaction between phenols and HONO, we first investigated the reaction at different pH values. We noted that the reaction kinetics are pH dependent, i.e., the formation rate of NO_2-BPA was much slower at higher pH values (pH > 5; Fig. 4D). This demonstrates that the formation of HONO at low pH is critical for the nitration of BPA [pK_a of HONO is ~3.27 (*41*)]. However, the pH of indoor surface reservoirs remains largely unknown and is likely to vary across the different indoor surfaces and conditions [e.g., mixing ratios of dominant acids and bases, such as CO_2 and NH_3 (*42*), and the use of acidic cleaning agents (*40*)]. Future studies are warranted to measure indoor surface pH and investigate its impacts on the nitration kinetics of BPA (*43*). We note that the reaction will proceed faster on acidic surfaces but nevertheless also occurs under alkaline conditions. Notably, nitroso-BPA (NO-BPA; m/z = 256.0973, retention time = 2.63 min) was detected in the reaction product mixture at ~100-fold lower abundance than NO_2-BPA in the aforementioned aqueous reaction. Therefore, we attempted to isolate the NO-BPA using high-performance liquid chromatography (HPLC) fractionation, but it was unsuccessful because of the rapid oxidation of NO-BPA to NO_2-BPA during purification. To check whether NO-BPA is a key intermediate to form NO_2-BPA, we performed the reaction between nitrite and BPA in an air-free environment using nitrogen gas flow to prevent NO-BPA from oxidation. While the formation of NO-BPA slightly increased under nitrogen (Fig. 4E), a more pronounced decrease was observed for NO_2-BPA by over an order of magnitude from 267 to 11.0%. The results demonstrate that NO-BPA is not primarily responsible for the formation of NO_2-BPA as an intermediate. Otherwise, high amounts of NO-BPA should be accumulated in the absence of air. This demonstrated that air is essential for the formation of NO_2-BPA from BPA through HONO, and future studies are warranted to clarify the exact reaction mechanism.

Nitration is a ubiquitous transformation pathway for indoor contaminants

As phenolic compounds, including bisphenols, are an important class of compounds used for various indoor applications, including plasticizers, antioxidants, and personal care products, we further investigated whether nitration is a vital transformation pathway for a broader spectrum of indoor contaminants. To test this, we used nontargeted analysis with ^{15}N-labeled nitrite to systematically identify nitrated indoor contaminants (see the workflow in Fig. 5A). In brief, the ^{15}N-labeled nitrite was incubated with the extracts of pooled indoor dust at pH 3 for 24 hours. As ^{15}N-labeled nitrite was

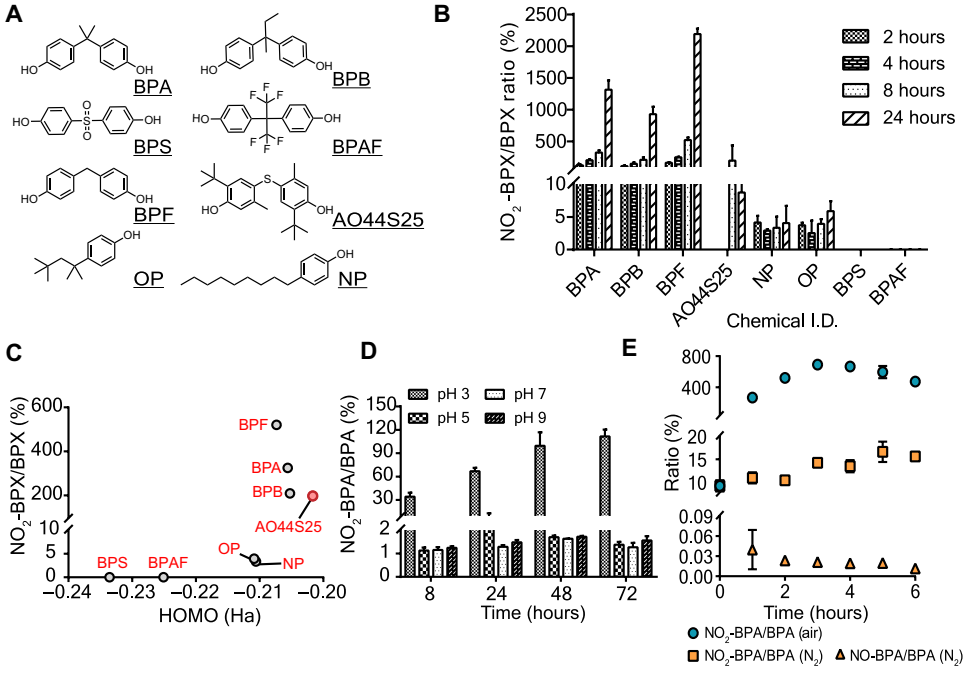

Fig. 4. The structure-related reaction of phenols with HONO in an aqueous solution. (**A**) Chemical structures of eight selected phenols. (**B**) The kinetics of nitration of eight compounds in 24 hours. (**C**) The relationship between the product ratios of eight compounds and their HOMO energies (in Hartrees). AO44S25 is labeled in red color because of the formation of the dinitration product. (**D**) The impact of pH on the kinetics of the aqueous nitration of BPA in 72 hours. Reaction is faster at pH below the pK_a (~3.27) of HONO. (**E**) The effect of air on the product ratio of NO-BPA and NO_2-BPA. NO-BPA data under air were not shown as NO-BPA was not detected. Data are presented from one representative experiment of three experiments performed with similar results.

used, the original ^{14}N-nitration compounds present in house dust can be discriminated against those that form in solution by their 0.9970-Da different *m/z* values. The ^{15}N-labeled reaction products were discriminated from background interferences by comparing the abundances of each LC-MS feature before and after the reaction. As shown in Fig. 5B, 110 peak features were detected after reaction with abundances >10-fold higher than the dust extract before reaction ($P < 0.05$). Because the nitrated compounds have never been reported before or recorded in the database, we established a new in silico database for nitrated transformation products by adding one (nitration, [M + NO_2-H]) or two NO_2 {dinitration, [M + 2(NO_2)-2H]} to the original TSCA compounds. The new in silico database was then used for database matching within a mass tolerance of 2 ppm. Among 110 LC-MS features, 60 compounds, including NO_2-BPA (searched in BPA form, [272.0930-NO_2]$^-$), returned at least one hit from the database searching (see Supplementary Data). Not unexpectedly, 71.4% of the nitration products are compounds with an aromatic substructure (Fig. 5C). Distinct aromatic substructures were detected for these 60 products, including phenols (37.9%), benzaldehyde (27.7%), benzene thiol (10.6%), aniline (6.75%), and benzoic acid (18.0%). These compounds demonstrated distinct kinetics over the 24-hour reaction course, which can be clustered into four different groups (Fig. 5D). In general, most of the compounds in groups 1 to 3 showed a continuous increase in abundance with increasing reaction time, while a few compounds in group 4 showed a decrease in abundance after 8-hour reactions. This demonstrated the high reactivity of group 4 compounds, which might form dinitration products after 8 hours, similar to AO44S25.

The detection of 110 ^{15}N-nitration reaction products provided an opportunity to retrospectively analyze the high-resolution mass spectra to detect ^{14}N-nitration products already present in the same house dust, i.e., before reaction. To achieve this, we searched ^{14}N analogs by matching *m/z* ([M-0.9970]) and retention times. Twelve ^{14}N analogs were detected in the same house dust extract, including NO_2-BPA (Fig. 5E and Supplementary Data), whose identities were supported by similar chromatographic profiles to ^{15}N-nitration products. Among these compounds, two highly abundant nitration products were assigned as the nitration and dinitration products from 4-*tert*-butylphenol, a widely applied antioxidant in plasticizer, surfactant, and commodity additives (Fig. 5E) (*44*). The detection of the 12 ^{14}N-nitration products demonstrates nitration with HONO as a reaction pathway for a broad spectrum of indoor aromatic pollutants. Future studies are warranted to investigate the occurrence of these 110 potential nitration products in more house dust samples.

DISCUSSION

Because of the immense number of indoor contaminants and their structural diversity, our understanding of indoor transformations remains largely incomplete (*13*). This study proposes a new top-down strategy to address research needs by combining protein-guided affinity purification, nontargeted analysis, and chemical transformation experiments to identify previously unknown indoor transformation products in an unbiased manner. We used the ERRγ protein as the "bait" to isolate its ligands from indoor dust extracts. A previously unknown ERRγ ligand was isolated from numerous background LC-MS peak features and confirmed as NO_2-BPA. By using an array of biophysical methods and reporter cells, NO_2-BPA was demonstrated to have strong physical and bioactive interactions with ERRγ. BPA has been widely reported to induce the malformation

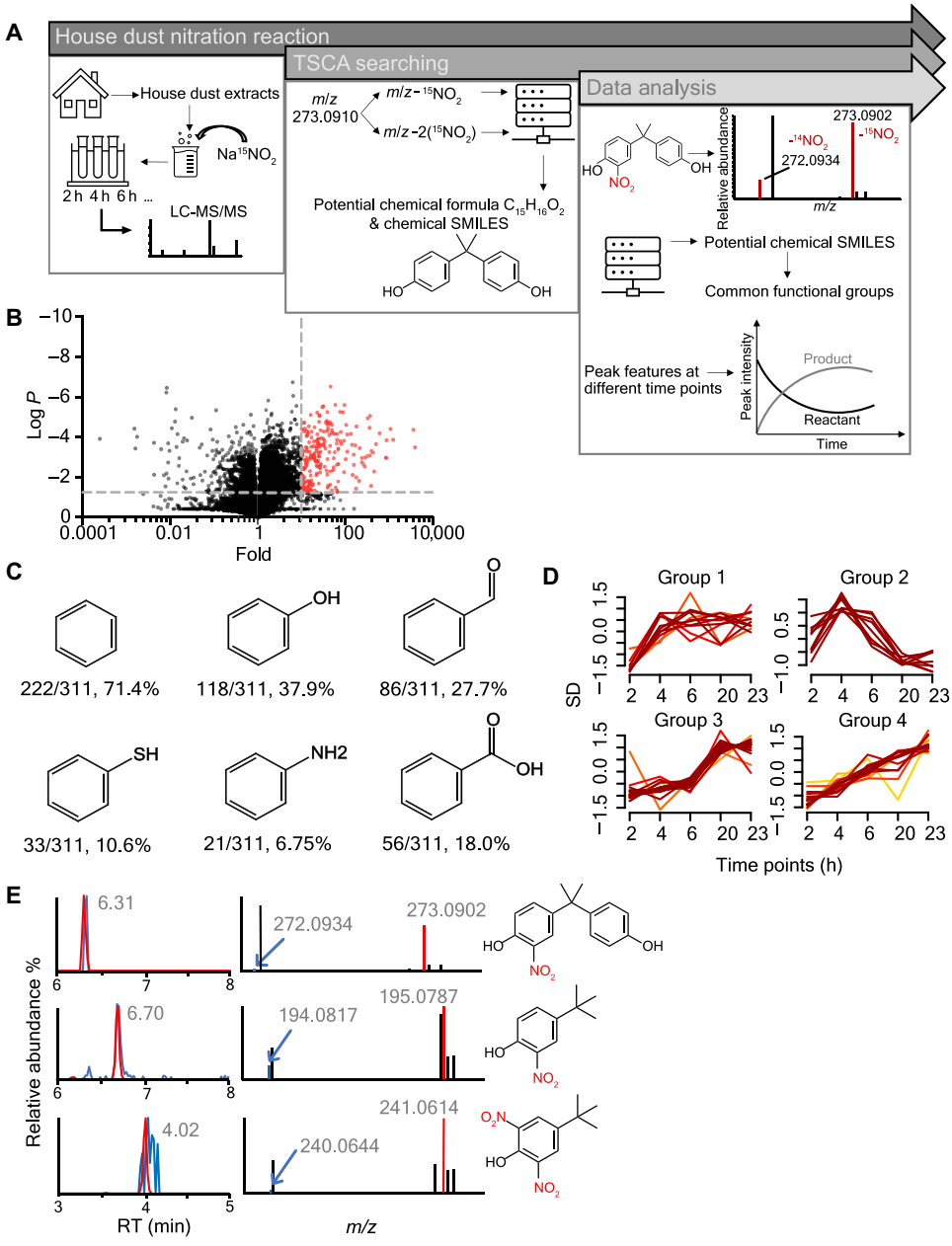

Fig. 5. Nitration of a broad spectrum of indoor contaminants. (**A**) The flowchart of in situ ^{15}N-nitrite labeling. The workflow is composed of three major steps: the ^{15}N-nitration of house dust extracts, the detection of LC-MS peak features and searching against an in silico database including the predicted nitration products of all TSCA compounds, and retrospectively analyzing the ^{14}N analogs. SMILES, simplified molecular-input line-entry system. (**B**) Volcano plot representing the log-transformed ratios and corresponding *P* values of peak features detected by LC-MS after reaction. The horizontal gray line shows the cutoff of the fold change between nitrated samples and negative controls (fold > 10). The vertical line indicates the cutoff of the log *P* values (–log *P* > 1.30). (**C**) The common substructures of nitrated contaminants. (**D**) Clustering of nitration compounds into four groups according to their LC-MS intensity changes over 23 hours. (**E**) Representative chromatogram, mass spectra (*m/z*), and tentative chemical structure of compounds detected in ^{14}N- and ^{15}N-nitrated forms with the same retention time (minutes). Blue color indicates the ^{14}N-nitrated form of compounds, while red indicates the ^{15}N-nitrated form. The chromatogram, mass spectrum, and chemical structure of NO_2-BPA are shown in the top, and the nitration and dinitration of 4-*tert*-butylphenol are shown in the middle and bottom, respectively.

of embryos and proliferation of breast cancer cells through ERRγ (*45*, *46*), and further investigations are warranted to investigate the ERRγ-mediated toxicological effects of NO_2-BPA. While the current study was focused on ERRγ and bisphenols, the same strategy can be applied to many other proteins (e.g., nuclear receptors) and indoor contaminants.

The discovery of nitration by HONO as a ubiquitous chemical transformation mechanism for indoor contaminants is significant at several levels. (i) In addition to binding to ERRγ, it is well known that nitroaromatic compounds are highly mutagenic (*47*). Most mutagenic and carcinogenic hazards of indoor house dusts remain unexplained by known compounds (*48*). Future studies are warranted

to clarify the potential contribution of nitration products to the mutagenicity of indoor dust mixtures. (ii) Bisphenols are a significant class of indoor contaminants used for many applications. While previous toxicological studies were focused on the parent compounds, the current study highlights the need to investigate the toxicities of their indoor transformation products. (iii) This work highlights the chemistry that arises from the presence of high levels of indoor gas-phase HONO. Whereas the heterogeneous reaction between HONO and surface-deposited nicotine has been investigated (*21*), this study demonstrates that HONO is involved in a broader range of additional chemical transformations in indoor environments.

MATERIALS AND METHODS

Chemicals and reagents

BPA, BPB, BPS, BPF, BPAF, AO44S25, 4-OP, 4-NP, 4OH-TAM, sodium nitrite-^{15}N, and SYPRO Orange dye were purchased from Sigma-Aldrich (Oakville, ON, Canada). HisPur Ni-NTA (nitrilotriacetic acid) magnetic beads and Zeba 7K spin desalting plates were purchased from Thermo Fisher Scientific (Whitby, ON, Canada). Human ERRγ open reading frame (ORF) clone (BC064700.1) and pET28-MHL vector were provided by Structural Genomics Consortium. BL21(DE3) competent *E. coli* was obtained from BioLabs Inc. (Whitby, ON, Canada). Antibody to histidine was purchased from Bioshop (Burlington, ON, Canada; TAG001.100) and was diluted with 5% skim milk at a dilution of 1:1000 for Western blotting. Horseradish peroxidase–linked anti-mouse immunoglobulin G secondary antibody (7076S) was purchased from Cell Signaling Technology (Beverly, Massachusetts, USA), which was used at a dilution of 1:20,000 in 5% skim milk.

Overexpression of ERRγ

The protein overexpression and purification were conducted according to Thouennon *et al.* (*49*). Briefly, the ERRγ ORF gene was cloned into pDB-His-GST plasmid and overexpressed in BL21 (DE3) *E. coli* cells as a tobacco etch virus (TEV)-cleavable 6×histidine-tagged fusion protein. The cells were first cultured on the LB plate and then aliquoted a single colony into LB media to culture overnight at 37°C. The bacteria cells were suspended with lysis buffer [10 mM tris-HCl (pH 7.5), 500 mM NaCl, 5% glycerol, and protease inhibitor cocktail tablet]. The resuspended cells were sonicated by a cell sonicator followed by centrifugation at 14,000*g* for 30 min. The supernatant containing the His-tagged ERRγ protein was transferred to new tubes and stored in a −80°C freezer for later use.

Protein affinity pulldown assay

The His-tagged ERRγ proteins were overexpressed in BL21 (DE3) *E. coli*. The protein affinity pulldown assay was conducted according to Peng *et al.* (*29*). The crude lysate of *E. coli*–overexpressed His-tagged ERRγ proteins (6 mg/liter) and the house dust extracts (diluted 100-fold) were added into the reaction buffer [50 mM tris-HCl, 150 mM NaCl, and 1 mM dithiothreitol (pH 8.0)] ($n = 3$). The wild-type *E. coli* with house dust extracts were treated as negative controls ($n = 3$). The extracts were incubated with protein solutions and then were aliquoted into a 96-well plate and incubated at 4°C for 1 hour. The HisPur Ni-NTA magnetic beads were added to each well to set on ice for 1 hour, and then we placed the plate on a magnetic separator and removed the supernatant. The beads were washed three times with wash buffer [20 mM tris-HCl (pH 8.2), 300 mM NaCl, and 10 mM imidazole], and the protein-ligand complexes were eluted using the elute buffer [20 mM tris-HCl (pH 8.2), 300 mM NaCl, and 300 mM imidazole]. The elutes were then transferred to a spin desalting plate to remove the nonspecifically bound compounds, followed by a denaturing process with 80% methanol.

Small-molecule analysis with HPLC-Orbitrap

The nontargeted analysis was conducted using Q Exactive MS equipped with a Vanquish UHPLC system. The injection volume was 2 μl. The C18 column (90 Å, 2.7 μm, 2.1 mm by 100 mm, HALO) was used to separate the chemicals. Two sets of mobile phases were used to analyze different compounds. Ultrapure water (A) and HPLC gradient methanol (B) were applied when analyzing NO_2-BPA, BPA, NO-BPA, BPS, 4-OP, 4-NP, and nitration house dust extracts. Ammonium hydroxide (0.03%) in both ultrapure water (A) and methanol (B) were used to analyze BPB, BPF, BPAF, and AO44S25. The HPLC gradients were the same for both sets of mobile phases, which were set to start with 10% of B and increase to 100% at 7 min to hold static for 3.5 min. This was followed by decreasing to 10% in 0.5 min and holding static for 1 min to reach equilibrium. The flow rate is 0.3 ml min^{-1}. The scan mode was combined with one full MS^1 scan followed by a data-independent acquisition (DIA) scan. The full MS^1 scanned *m/z* from 100 to 1000 in switch mode at resolution $R = 70{,}000$ (at *m/z* 200) with a collection of a maximum of 3×10^6 ions in 200 ms. Four DIA tandem MS (MS/MS) scans were set to cover the *m/z* from 150 to 450 and 450 to 750 in both negative and positive modes. The DIA scan was recorded at resolution $R = 35{,}000$ (at *m/z* 200) with a maximum of 1×10^5 ions collected within 60 ms. The data were collected using 10 *m/z* isolation windows per MS/MS scan. Therefore, in total, there were twenty 10 *m/z*–wide windows between 150 and 450 *m/z* and 450 and 750 *m/z*. Electrospray ionization source was used with the following parameters: 3 kV of spray voltage, 40 liters/hour of sheath gas flow rate, 5 liters/hour of auxiliary gas flow rate, and 300°C of capillary temperature.

Isothermal titration calorimetry

The ERRγ LBDs were purified and dissolved in 400 μl of 150 mM NaCl and 20 mM Hepes (pH 7.5) to reach the final concentration of 25 μM and then equilibrated for 1 hour at room temperature before ITC measurement. An Auto-iT200 calorimeter (Malvern Instruments) was used to conduct the measurements at 25°C. The concentration of NO_2-BPA was 200 μM, of which 2-μl aliquots were added automatically to the ERRγ LBDs in the calorimeter cell. NO_2-BPA (2 μl) was also added into the dissolving buffer to serve as the blank, and heat responses were subtracted. The negative control was conducted via injecting the vehicle solvent, 100% (v/v) dimethyl sulfoxide (DMSO), which was used to dissolve NO_2-BPA, into the protein solution with insignificant heats of dilution produced. Integrated heat effects were analyzed using Microcal Origin 7 software (Malvern Instruments).

Thermal shift assays

Thermofluor-type assay was used to determine the thermostabilities of ERRγ in the presence of chemicals. Briefly, 2 μl of 30 μM purified ERRγ LBDs was added into 96-well plates with the final concentration of 3 μM per well. NO_2-BPA was dissolved and serially diluted with 100% (v/v) DMSO and added into the well with 1% (v/v) DMSO in the final concentration of 25 μM ($n = 3$). Thermal shift

assay buffer (15 μl) was added into wells and then incubated at 4°C for 2 hours. Aliquot (2 μl) of 100-fold SYPRO Orange dye (Sigma-Aldrich) was added to each well, and then we sealed the wells. We gently rotated the wells to mix the protein and dye for 15 s and centrifuged the plates at 1000*g* for 1 min. QuantStudio 6 Flex Real-Time PCR System (Thermo Fisher Scientific) was used to measure the protein melting curves with the following program: 2 min at 25°C, ramp to 95°C at 1°C s^{-1}, and 2 min at 95°C, with excitation and emission wavelengths of 483 and 568 nm, respectively. The baseline T_m (melting transition temperature; T_{m0}) was defined on the basis of the melting temperature of the ERRγ solution without exposure to NO_2-BPA. The thermo-shift effects of compounds were obtained by plotting mean ΔT_{ms} ($T_{mligand} - T_{m0}$) versus ligand concentrations. A three-parameter dose-response nonlinear regression function was fit to the data using the GraphPad Prism v7 (GraphPad Software, La Jolla, CA).

LANCE nuclear receptor assay

LANCE-FRET coregulator buffer was freshly prepared before use [5 mM dithiothreitol, 10 mM Hepes, 150 mM NaCl, 0.005% Tween 20, and 0.1% fatty acid–free bovine serum albumin (pH 7.4)]. The 100× stock solutions of NO_2-BPA were prepared in 100% (v/v) DMSO and then diluted with LANCE-FRET coregulator buffer before adding to the 384-well plate. Eleven points of concentrations were prepared through threefold serial dilutions starting with the highest final concentration of 100 μM ($n = 3$). The stock solutions of 20 nM ERRγ LBD were prepared in cold LANCE-FRET coregulator buffer, and 2000 nM biotin-PGC1a, 8 nM Eu-W1024–labeled anti-6×His antibody, and 400 nM ULight-streptavidin were prepared in the buffer at room temperature. Five microliters of each stock solution was added to the plate. The 384-well plate was gently mixed on a plate shaker and then incubated at room temperature for 2 hours in a dark environment. The plate was read at wavelengths of 615 and 655 nm, using the instrument settings as follows: excitation filter (340 nm) and two emission filters (615 and 665 nm), the integration time of 200 μs, and a delay time of 100 μs. The 665/615 ratio was calculated and normalized to the negative control reaction using 1% (v/v) DMSO. The samples with the saturating dose of chemicals were treated as positive controls.

ERRγ reporter assay

The HG5LN GAL4-*h*ERRγ cells were used for the reporter assay. The cells were generated by transfecting HG5LN cells with the pSG5-GAL4(DBD)-*h*ERR(LBD)-puro plasmid, more details of which have been described in the work of Thouennon *et al.* (*49*). The cells were cultured in 96-well white opaque tissue culture plates with a density of 25,000 cells per well. To test the agonistic effects of NO_2-BPA, four points of concentration (0.3, 1, 3, and 10 μM, $n = 3$) of NO_2-BPA with 4OH-TAM (0.3 μM) were added into cell cultures after 24 hours of seeding and incubated for 16 hours at 37°C. The consistently activated ERRγ proteins were inhibited with 4OH-TAM before testing the bioactivity effect of NO_2-BPA. The cell culture medium was changed to Dulbecco's modified Eagle's medium/F12 medium (Invitrogen) with 0.3 mM luciferin. The luciferase signal was obtained from a MicroBeta Wallac luminometer (PerkinElmer). Statistical significance was determined using Student's *t* test.

Synthesis of NO_2-BPA

NO_2-BPA was synthesized using a simple aqueous reaction by mixing 0.02 g of BPA and 1.25 g of sodium nitrite ($NaNO_2$) in 50 ml of pure water at pH 6 for 6 hours. The reaction products were extracted by using 10 ml of ethyl acetate three times. The extracts were dried using the rotary evaporator. NO-BPA and dinitrated BPA were formed as minor products. To purify NO_2-BPA from the side products, we injected 500 μl of the reconstituted solution in methanol into HPLC (Agilent 1260 Infinity LC system with an ultraviolet detector) for separation. The fraction with NO_2-BPA only was confirmed by LC-MS/MS and NMR spectroscopy.

Molecular docking

The molecular modeling simulation software AutoDock4.0 was used to investigate the binding sites of NO_2-BPA to ERRγ. The method was referred to Forli *et al.* (*50*). The crystal structure of ERRγ (2E2R) was downloaded from the Protein Data Bank (PDB) website (www.rcsb.org/). The three-dimensional (3D) structure of NO_2-BPA was prepared in ChemDraw 3D. The cocrystallized BPA and all water molecules were removed from the original PDB coordinate file. The grid box was centered at the macromolecule, and the number of points in *x*, *y*, and *z* dimensions was 108 × 92 ×112, correspondingly including the entire protein structure. The parameters of the genetic algorithm (GA) of docking were set as default, except that the number of GA runs was changed to 50. The results of molecular docking were visualized using PyMOL.

House dust sample collection

Ten house dust samples were collected in different houses in Toronto, Canada, for pulldown experiments. Another 31 house dust samples were collected to determine the ubiquitous occurrence of NO_2-BPA. The extraction procedures were the same for all house dust samples. Briefly, a clean vacuum cleaner was used to collect dust samples in different houses. The entire floor area was covered by the vacuum cleaner in each house. To reduce cross-contamination, the vacuum cleaner was cleaned with water and left to dry for at least 1 day before the next use. The samples collected were first removed of all the large components, such as papers and hairs. Dust (~0.01 g) was weighted from each sample and transferred to a 15-ml Falcon tube. The samples were extracted with 4 ml of methanol with vigorous shaking for 30 min followed by 30 min of sonication. The falcon tubes were centrifuged at 4000*g* for 10 min. The supernatant was carefully transferred to a new tube, followed by blowing to dryness with nitrogen. The samples were reconstituted with 200 μl of 50% (v/v) methanol and centrifuged at 14,000*g* for 10 min to remove the insoluble chemicals. The supernatants were transferred to a new 1.5-ml tube and stored at −20°C for the pulldown assay. To assess the recovery, 570 ng of BPA and 137 ng of NO_2-BPA were spiked to ~0.01 g of house dusts ($n = 6$). The samples were incubated in the dark for 24 hours to allow for equilibrium before the extraction. The recoveries of BPA and NO_2-BPA were determined to be 75.6 ± 9.4 and 69.5 ± 7.2%, respectively.

Heterogeneous dark HONO reactions

$NaNO_2$-coated glass tube

The $NaNO_2$ coating solution was made by mixing 0.3 g of $NaNO_2$ (Sigma-Aldrich, product no. 563218) with 3 ml of methanol (Sigma-Aldrich, product no. 34860). The mixture solution was transferred into a glass tube (inner diameter of 6.4 mm, outer diameter of 9.6 mm, and length of 81.3 cm) via a pipette (VWR) and was dried by passing air (flow rate of 100 cm^3 min^{-1}) through the tube. After the complete evaporation of methanol, the dried solid $NaNO_2$ was coated on the surface of the glass tube.

Generation of gaseous HONO

The solid $NaNO_2$ (coated on the glass tube) was exposed to a flow of zero air (flow rate of 100 cm^3 min^{-1}) bubbling through a HCl solution (0.65 M HCl in ultrapure water), resulting in the formation of gaseous HONO (*51*, *52*)

$$NaNO_2(s) + HCl(g) \rightarrow NaCl(s) + HONO(g) \quad (1)$$

The HONO-containing flow was mixed with another zero air flow before entering the flow tube reactor (fig. S3A).

To verify whether the HCl vapor entering the $NaNO_2$-coated glass tube is completely consumed, we add another $NaNO_2$-coated glass tube to the HONO generation system (see fig. S3B). In this case, if the HCl vapor entering the first glass tube is completely consumed, then there should be no significant difference between the measured HONO concentration in the two-tube system ($HONO_{two\text{-}tube}$) and the measured HONO concentration in the one-tube system ($HONO_{one\text{-}tube}$), i.e., $HONO_{two\text{-}tube} \approx HONO_{one\text{-}tube}$. Conversely, if the HCl entering the first glass tube is not completely consumed, then the remaining HCl will react with the $NaNO_2$ coated on the second glass tube, leading to a higher HONO concentration, i.e., $HONO_{two\text{-}tube} > HONO_{one\text{-}tube}$. The experimental results suggest that the HONO concentration is relatively stable, regardless of the use of different HONO generation systems. This indicates that, under the current experimental conditions, HCl vapor is completely consumed within the first $NaNO_2$-coated glass tube. Thus, the airflow entering the flow tube reactor should contain negligible HCl.

Detection of HONO

The gaseous HONO concentration was indirectly measured with a chemiluminescence NO_x analyzer ($NO_x = NO + NO_2$; Thermo Fisher Scientific, model 42i) as described below. In this method, NO concentration is measured by oxidizing NO with internally generated O_3 to produce excited-state NO_2^*, which further relaxes to the ground state by emitting a photon (*53*). The intensity of the characteristic luminescence is proportional to the concentration of NO originally oxidized

$$NO + O_3 \rightarrow NO_2^* + O_2 \quad (2)$$

$$NO_2^* \rightarrow NO_2 + h\nu \quad (3)$$

For the detection of NO_2, NO_2 is reduced to NO by a molybdenum (Mo) NO_2-to-NO converter so that the concentration of NO_2 can be quantified using the abovementioned chemiluminescent approach (*53*). Note that Mo catalysts are also known to efficiently reduce HONO (*54*). Thus, when HONO is present in the sample airflow, it is reported by the instrument as NO_2

$$\text{Measured } NO_2 = NO_2 + HONO \quad (4)$$

To quantify the concentration of HONO, we add a Na_2CO_3 denuder (0.2 g of Na_2CO_3 coated on the surface of a glass tube; inner diameter of 6.4 mm, outer diameter of 9.6 mm, and length of 82.3 cm) to the sampling line between the exit of the flow tube reactor and the NO_x analyzer (fig. S1A) to remove HONO from the flow. As shown in fig. S4A, HONO is efficiently trapped in the Na_2CO_3 denuder and can be indirectly quantified from the difference between the NO_2 signals with and without the denuder

$$\begin{aligned} HONO = {} & \text{Measured } NO_2(\text{without } Na_2CO_3 \text{ denuder}) \\ & - \text{Measured } NO_2(\text{with } Na_2CO_3 \text{ denuder}) \end{aligned} \quad (5)$$

This indirect HONO detection technique has been widely used in previous laboratory studies (*55*–*57*). Here, given that the NO_2 mixing ratio in the background zero air is ~0 ppb (fig. S4A), all the reported NO_2 in the flow exiting the flow tube reactor can be considered to be HONO.

Coating of BPX (BPA, BPB, and BPS) on glass surfaces

A 150-μl aliquot of BPA solution (17.6 mM BPA in methanol) was pipetted onto a circular microscope cover glass (diameter of 25 mm; Thermo Fisher Scientific; product no. 12545102), resulting in an average BPA coating thickness of 1 nm after the evaporation of methanol in zero air; it is unlikely that the coatings are uniform. The BPB and BPS samples were prepared using the same approach. Five BPX-coated glasses were aligned on a Teflon holder with an approximately 3-cm distance separation. The Teflon holder was placed inside a flow tube reactor.

Flow tube experiments

The heterogeneous reactions between gaseous HONO and BPX coated on the glasses were investigated using a dark glass flow tube reactor (inner diameter of 6.4 cm, outer diameter of 6.8 cm, and length of 1.48 m), with the experimental setup given in fig. S3A. The total flow rate through the flow tube reactor was 0.8 liters min^{-1}, with a residence time of 6 min. The relative humidity (RH) in the flow tube was constantly maintained at a selected value (10 and 50% RH) by varying the ratio of dry to wet zero air, as measured with a hygrometer (Vaisala, model M170). The HONO mixing ratio was relatively stable within the 6-hour reaction, as shown in fig. S4B. The heterogeneous reaction experiment was halted after 6 hours of HONO exposure. We then replaced the used $NaNO_2$-coated glass tube with a new $NaNO_2$-coated tube and started the second 6-hour HONO reaction experiment. As a result, the total HONO exposure time was 12 hours (6 + 6 hours). After 12 hours of reaction, each reacted BPX sample was immediately extracted with 1 ml of methanol containing bis(2-ethylhexyl) sebacate (1 μM; used as an internal standard) for subsequent LC analysis.

Aqueous-phase nitration of aromatic phenols and house dust extractions

For the aqueous-phase nitration of aromatic compounds, eight aromatic phenols were selected: BPA, BPB, BPS, BPF, BPAF, AO44S25, 4-OP, and 4-NP. The chemical mixtures were diluted with phosphate-buffered saline (PBS) solution with different pH values (pH 3, 5, 7, and 9), and $NaNO_2$ was added with a final concentration of 10 mM. The samples were shaken in a dark environment, and then we collected 5 μl of samples at 2, 4, 8, 16, 20, 24, and 48 hours. Similarly, for the ^{15}N-nitration of house dust extracts, the extracts were diluted 10-fold with pH-adjusted PBS buffer (pH 3). The isotopically labeled $Na^{15}NO_2$ was added to the house dust extract solution with a final concentration of 50 mM ($n = 3$). The samples were placed in a dark environment to shake and react. Five microliters of each solution was collected at 2, 4, 6, 20, and 23 hours and diluted 100-fold in methanol with 0.5% (v/v) ammonium hydroxide.

Nontargeted/suspect data analysis

The nontargeted data analysis was performed via an in-house R algorithm. The raw files produced by the instrument were converted to mzXML format. The XCMS package was used to detect the LC-MS

peaks in the files with a mass tolerance of 2 ppm (*37*). The retention time adjustment was made before searching for the LC-MS peak features matched across samples with a mass tolerance of 2 ppm and a retention time window of 20 s. Two screening processes were conducted to further analyze LC-MS peak features: (i) calculate the ratio of peak abundances between treated samples (in the presence of ERRγ) and negative controls (in the absence of ERRγ) and (ii) determine the significance of the difference between the treated samples and negative controls. To be specific, for the pulldown experiment, the ratio of abundances of house dust extract–treated ERRγ samples to those without extract exposure was calculated for each peak feature.

In addition, for the nitration reaction of house dust extracts, the ratio of abundances of $Na^{15}NO_2$-treated house dust extracts to those without chemically treated samples was calculated for peak features. The *P* value of the difference between them was calculated through a *t* test. After these calculations, the peak features that fulfilled the criteria, a ratio greater than 10 and a *P* value less than 0.05, were selected to perform subsequent data analysis. The final differentiated peak list obtained from the R program was manually checked using MS^1 *m/z* and retention time. For the pulldown experiment, there was only one unknown LC-MS peak feature (*m/z* = 272.0930) that complied with the criteria. The chemical structure was confirmed with the MS^2 spectrum and a synthesized chemical standard. For the nitration of house dust experiment, the *m/z* values of nitrated ([M + NO_2-H]) and dinitrated ([M + 2(NO_2)-2H]) compounds were first searched against an in silico database for nitration products. The new in silico database was established by adding one or two nitro groups to all compounds in the TSCA Chemical Substance Inventory provided by the U.S. Environmental Protection Agency (www.epa.gov/tsca-inventory). The new in silico database was used for database matching to the 110 LC-MS features within a mass tolerance of 2 ppm, followed by data analysis, which was composed of three steps: (i) distinguish the ^{15}N-labeled nitrated compounds from the originally existing ^{14}N-nitrated compounds in the dust samples and determine their ratio, (ii) summarize the returned chemical structures from the in silico database and classify these compounds' common functional subgroups, and (iii) plot the kinetics of the compounds to demonstrate the production of nitrated products in the aqueous reaction.

Computational methods

Density functional theory (DFT) calculations were conducted with Gaussian 16. The geometry optimizations were performed at B3LYP level of DFT with the 6-311G (d,p) basis set. Molecular orbital energies of the eight phenols were estimated by B3LYP/6-31G(d) level of theory.

SUPPLEMENTARY MATERIALS

Supplementary material for this article is available at https://science.org/doi/10.1126/sciadv.abq7023

REFERENCES AND NOTES

1. F. Mercier, P. Glorennec, O. Thomas, B. Le Bot, Organic contamination of settled house dust, a review for exposure assessment purposes. *Environ. Sci. Technol.* **45**, 6716–6727 (2011).
2. A. H. Goldstein, W. W. Nazaroff, C. J. Weschler, J. Williams, How do indoor environments affect air pollution exposure? *Environ. Sci. Technol.* **55**, 100–108 (2021).
3. B. Yuan, J. H. Tay, J. A. Padilla-Sánchez, E. Papadopoulou, L. S. Haug, C. A. de Wit, Human exposure to chlorinated paraffins via inhalation and dust ingestion in a Norwegian cohort. *Environ. Sci. Technol.* **55**, 1145–1154 (2021).
4. D. Chen, K. Kannan, H. Tan, Z. Zheng, Y. L. Feng, Y. Wu, M. Widelka, Bisphenol analogues other than BPA: Environmental occurrence, human exposure, and toxicity—A review. *Environ. Sci. Technol.* **50**, 5438–5453 (2016).
5. A. Shankar, S. Teppala, C. Sabanayagam, Bisphenol A and peripheral arterial disease: Results from the NHANES. *Environ. Health Perspect.* **120**, 1297–1300 (2012).
6. I. A. Lang, T. S. Galloway, A. Scarlett, W. E. Henley, M. Depledge, R. B. Wallace, D. Melzer, Association of urinary bisphenol A concentration with medical disorders and laboratory abnormalities in adults. *JAMA* **300**, 1303–1310 (2008).
7. S. N. Loganathan, K. Kannan, Occurrence of bisphenol A in indoor dust from two locations in the eastern United States and implications for human exposures. *Arch. Environ. Contam. Toxicol.* **61**, 68–73 (2011).
8. C. Liao, F. Liu, Y. Guo, H. B. Moon, H. Nakata, Q. Wu, K. Kannan, Occurrence of eight bisphenol analogues in indoor dust from the United States and several Asian countries: Implications for human exposure. *Environ. Sci. Technol.* **46**, 9138–9145 (2012).
9. H. Peng, D. M. V. Saunders, J. X. Sun, P. D. Jones, C. K. C. Wong, H. L. Liu, J. P. Giesy, Mutagenic azo dyes, rather than flame retardants, are the predominant brominated compounds in house dust. *Environ. Sci. Technol.* **50**, 12669–12677 (2016).
10. K. Hoffman, S. Garantziotis, L. S. Birnbaum, H. M. Stapleton, Monitoring indoor exposure to organophosphate flame retardants: Hand wipes and house dust. *Environ. Health Perspect.* **123**, 160–165 (2015).
11. C. D. Kassotis, K. Hoffman, H. M. Stapleton, Characterization of adipogenic activity of house dust extracts and semi-volatile indoor contaminants in 3T3-L1 cells. *Environ. Sci. Technol.* **51**, 8735–8745 (2017).
12. J. P. D. Abbatt, C. Wang, The atmospheric chemistry of indoor environments. *Environ Sci Process Impacts* **22**, 25–48 (2020).
13. S. Gligorovski, J. P. D. Abbatt, An indoor chemical cocktail. *Science* **359**, 632–633 (2018).
14. C. J. Weschler, Chemistry in indoor environments: 20 years of research. *Indoor Air* **21**, 205–218 (2011).
15. W. Wang, M. J. Ezell, P. S. J. Lakey, K. Z. Aregahegn, M. Shiraiwa, B. J. Finlayson-Pitts, Unexpected formation of oxygen-free products and nitrous acid from the ozonolysis of the neonicotinoid nitenpyram. *Proc. Natl. Acad. Sci. U.S.A.* **117**, 11321–11327 (2020).
16. C. J. Weschler, N. Carslaw, Indoor chemistry. *Environ. Sci. Technol.* **52**, 2419–2428 (2018).
17. W. A. Pryor, B. Das, D. F. Church, The ozonation of unsaturated fatty acids: Aldehydes and hydrogen peroxide as products and possible mediators of ozone toxicity. *Chem. Res. Toxicol.* **4**, 341–348 (1991).
18. A. Wisthaler, C. J. Weschler, Reactions of ozone with human skin lipids: Sources of carbonyls, dicarbonyls, and hydroxycarbonyls in indoor air. *Proc. Natl. Acad. Sci. U.S.A.* **107**, 6568–6575 (2010).
19. Z. L. Zhou, J. P. D. Abbatt, Formation of gas-phase hydrogen peroxide via multiphase ozonolysis of unsaturated lipids. *Environ. Sci. Technol. Lett.* **8**, 114–120 (2021).
20. Y. Liu, P. K. Misztal, C. Arata, C. J. Weschler, W. W. Nazaroff, A. H. Goldstein, Observing ozone chemistry in an occupied residence. *Proc. Natl. Acad. Sci. U.S.A.* **118**, e2018140118 (2021).
21. M. Sleiman, L. A. Gundel, J. F. Pankow, P. Jacob III, B. C. Singer, H. Destaillats, Formation of carcinogens indoors by surface-mediated reactions of nicotine with nitrous acid, leading to potential thirdhand smoke hazards. *Proc. Natl. Acad. Sci. U.S.A.* **107**, 6576–6581 (2010).
22. D. B. Collins, R. F. Hems, S. Zhou, C. Wang, E. Grignon, M. Alavy, J. A. Siegel, J. P. D. Abbatt, Evidence for gas-surface equilibrium control of indoor nitrous acid. *Environ. Sci. Technol.* **52**, 12419–12427 (2018).
23. S. Zhou, C. J. Young, T. C. VandenBoer, S. F. Kowal, T. F. Kahan, Time-resolved measurements of nitric oxide, nitrogen dioxide, and nitrous acid in an occupied New York home. *Environ. Sci. Technol.* **52**, 8355–8364 (2018).
24. R. S. Judson, K. A. Houck, R. J. Kavlock, T. B. Knudsen, M. T. Martin, H. M. Mortensen, D. M. Reif, D. M. Rotroff, I. Shah, A. M. Richard, D. J. Dix, In vitro screening of environmental chemicals for targeted testing prioritization: The ToxCast Project. *Environ. Health Perspect.* **118**, 485–492 (2010).
25. Z. Y. Wang, G. W. Walker, D. C. G. Muir, K. Nagatani-Yoshida, Toward a global understanding of chemical pollution: A first comprehensive analysis of national and regional chemical inventories. *Environ. Sci. Technol.* **54**, 2575–2584 (2020).
26. J. Han, S. Wang, K. Yeung, D. Yang, W. Gu, Z. Ma, J. Sun, X. Wang, C. W. Chow, A. W. H. Chan, H. Peng, Proteome-wide effects of naphthalene-derived secondary organic aerosol in BEAS-2B cells are caused by short-lived unsaturated carbonyls. *Proc. Natl. Acad. Sci. U.S.A.* **117**, 25386–25395 (2020).
27. D. M. Cwiertny, S. A. Snyder, D. Schlenk, E. P. Kolodziej, Environmental designer drugs: When transformation may not eliminate risk. *Environ. Sci. Technol.* **48**, 11737–11745 (2014).

28. B. I. Escher, K. Fenner, Recent advances in environmental risk assessment of transformation products. *Environ. Sci. Technol.* **45**, 3835–3847 (2011).
29. H. Peng, J. Sun, H. A. Alharbi, P. D. Jones, J. P. Giesy, S. Wiseman, Peroxisome proliferator-activated receptor γ is a sensitive target for oil sands process-affected water: Effects on adipogenesis and identification of ligands. *Environ. Sci. Technol.* **50**, 7816–7824 (2016).
30. D. W. Yang, J. J. Han, D. R. Hall, J. X. Sun, J. Fu, S. Kutarna, K. A. Houck, C. A. LaLone, J. A. Doering, C. A. Ng, H. Peng, Nontarget screening of per- and polyfluoroalkyl substances binding to human liver fatty acid binding protein. *Environ. Sci. Technol.* **54**, 5676–5686 (2020).
31. W. X. Hu, Y. T. Jia, Q. Y. Kang, H. Peng, H. J. Ma, S. Y. Zhang, Y. H. Hiromori, T. Kimura, T. Nakanishi, L. M. Zheng, Y. F. Qiu, Z. B. Zhang, Y. Wan, J. Y. Hu, Screening of house dust from Chinese homes for chemicals with liver X receptors binding activities and characterization of atherosclerotic activity using an in vitro macrophage cell line and ApoE$^{-/-}$ mice. *Environ. Health Perspect.* **127**, 117003 (2019).
32. J. Misra, D. K. Kim, H. S. Choi, ERRγ: A junior orphan with a senior role in metabolism. *Trends Endocrinol. Metab.* **28**, 261–272 (2017).
33. D. K. Kim, J. R. Kim, M. Koh, Y. D. Kim, J. M. Lee, D. Chanda, S. B. Park, J. J. Min, C. H. Lee, T. S. Park, H. S. Choi, Estrogen-related receptor γ (ERRγ) is a novel transcriptional regulator of phosphatidic acid phosphatase, LIPIN1, and inhibits hepatic insulin signaling. *J. Biol. Chem.* **286**, 38035–38042 (2011).
34. D. K. Kim, Y. H. Kim, H. H. Jang, J. Park, J. R. Kim, M. Koh, W. I. Jeong, S. H. Koo, T. S. Park, C. H. Yun, S. B. Park, J. Y. L. Chiang, C. H. Lee, H. S. Choi, Estrogen-related receptor γ controls hepatic CB1 receptor-mediated CYP2E1 expression and oxidative liver injury by alcohol. *Gut* **62**, 1044–1054 (2013).
35. S. Takayanagi, T. Tokunaga, X. Liu, H. Okada, A. Matsushima, Y. Shimohigashi, Endocrine disruptor bisphenol A strongly binds to human estrogen-related receptor gamma (ERRgamma) with high constitutive activity. *Toxicol. Lett.* **167**, 95–105 (2006).
36. U.S. EPA, TSCA Chemical Substance Inventory (2018); www.epa.gov/tsca-inventory.
37. S. Kutarna, S. Tang, X. Hu, H. Peng, Enhanced nontarget screening algorithm reveals highly abundant chlorinated azo dye compounds in house dust. *Environ. Sci. Technol.* **55**, 4729–4739 (2021).
38. K. Vidović, D. Lašič Jurković, M. Šala, A. Kroflič, I. Grgić, Nighttime aqueous-phase formation of nitrocatechols in the atmospheric condensed phase. *Environ. Sci. Technol.* **52**, 9722–9730 (2018).
39. T. Vasiljevic, T. Harner, Bisphenol A and its analogues in outdoor and indoor air: Properties, sources and global levels. *Sci. Total Environ.* **789**, 148013 (2021).
40. C. Wang, D. B. Collins, C. Arata, A. H. Goldstein, J. M. Mattila, D. K. Farmer, L. Ampollini, P. F. DeCarlo, A. Novoselac, M. E. Vance, W. W. Nazaroff, J. P. D. Abbatt, Surface reservoirs dominate dynamic gas-surface partitioning of many indoor air constituents. *Sci. Adv.* **6**, eaay8973 (2020).
41. E. Riordan, N. Minogue, D. Healy, P. O'Driscol, J. R. Sodeau, Spectroscopic and optimization modeling study of nitrous acid in aqueous solution. *J. Phys. Chem. A* **109**, 779–786 (2005).
42. W. W. Nazaroff, C. J. Weschler, Indoor acids and bases. *Indoor Air* **30**, 559–644 (2020).
43. A. P. Ault, V. H. Grassian, N. Carslaw, D. B. Collins, H. Destaillats, D. J. Donaldson, D. K. Farmer, J. L. Jimenez, V. F. McNeill, G. C. Morrison, R. E. O'Brien, M. Shiraiwa, M. E. Vance, J. R. Wells, W. Xiong, Indoor surface chemistry: Developing a molecular picture of reactions on indoor interfaces. *Chem* **6**, 3203–3218 (2020).
44. R. Liu, Y. Lin, T. Ruan, G. Jiang, Occurrence of synthetic phenolic antioxidants and transformation products in urban and rural indoor dust. *Environ. Pollut.* **221**, 227–233 (2017).
45. M. Tohmé, S. M. Prud'homme, A. Boulahtouf, E. Samarut, F. Brunet, L. Bernard, W. Bourguet, Y. Gibert, P. Balaguer, V. Laudet, Estrogen-related receptor γ is an in vivo receptor of bisphenol A. *FASEB J.* **28**, 3124–3133 (2014).
46. H. Song, T. Zhang, P. Yang, M. Li, Y. Yang, Y. Wang, J. Du, K. Pan, K. Zhang, Low doses of bisphenol A stimulate the proliferation of breast cancer cells via ERK1/2/ERRγ signals. *Toxicol. In Vitro* **30**, 521–528 (2015).
47. V. Purohit, A. K. Basu, Mutagenicity of nitroaromatic compounds. *Chem. Res. Toxicol.* **13**, 673–692 (2000).
48. R. M. Maertens, R. W. Gagne, G. R. Douglas, J. P. Zhu, P. A. White, Mutagenic and carcinogenic hazards of settled house dust II: Salmonella mutagenicity. *Environ. Sci. Technol.* **42**, 1754–1760 (2008).
49. E. Thouennon, V. Delfosse, R. Bailly, P. Blanc, A. Boulahtouf, M. Grimaldi, A. Barducci, W. Bourguet, P. Balaguer, Insights into the activation mechanism of human estrogen-related receptor γ by environmental endocrine disruptors. *Cell. Mol. Life Sci.* **76**, 4769–4781 (2019).
50. S. Forli, R. Huey, M. E. Pique, M. F. Sanner, D. S. Goodsell, A. J. Olson, Computational protein-ligand docking and virtual drug screening with the AutoDock suite. *Nat. Protoc.* **11**, 905–919 (2016).
51. M. Lao, L. R. Crilley, L. Salehpoor, T. C. Furlani, I. Bourgeois, J. A. Neuman, A. W. Rollins, P. R. Veres, R. A. Washenfelder, C. C. Womack, C. J. Young, T. C. VandenBoer, A portable, robust, stable, and tunable calibration source for gas-phase nitrous acid (HONO). *Atmos. Meas. Tech.* **13**, 5873–5890 (2020).
52. A. Febo, C. Perrino, M. Gherardi, R. Sparapani, Evaluation of a high-purity and high-stability continuous generation system for nitrous acid. *Environ. Sci. Technol.* **29**, 2390–2395 (1995).
53. G. Villena, I. Bejan, R. Kurtenbach, P. Wiesen, J. Kleffmann, Interferences of commercial NO_2 instruments in the urban atmosphere and in a smog chamber. *Atmos. Meas. Tech.* **5**, 149–159 (2012).
54. E. J. Dunlea, S. C. Herndon, D. D. Nelson, R. M. Volkamer, F. San Martini, P. M. Sheehy, M. S. Zahniser, J. H. Shorter, J. C. Wormhoudt, B. K. Lamb, E. J. Allwine, J. S. Gaffney, N. A. Marley, M. Grutter, C. Marquez, S. Blanco, B. Cardenas, A. Retama, C. R. R. Villegas, C. E. Kolb, L. T. Molina, M. J. Molina, Evaluation of nitrogen dioxide chemiluminescence monitors in a polluted urban environment. *Atmos. Chem. Phys.* **7**, 2691–2704 (2007).
55. M. E. Monge, B. D'Anna, L. Mazri, A. Giroir-Fendler, M. Ammann, D. J. Donaldson, C. George, Light changes the atmospheric reactivity of soot. *Proc. Natl. Acad. Sci. U.S.A.* **107**, 6605–6609 (2010).
56. H. Schwartz-Narbonne, S. H. Jones, D. J. Donaldson, Indoor lighting releases gas phase nitrogen oxides from indoor painted surfaces. *Environ. Sci. Technol. Lett.* **6**, 92–97 (2019).
57. C. Han, W. Yang, Q. Wu, H. Yang, X. Xue, Heterogeneous photochemical conversion of NO2 to HONO on the humic acid surface under simulated sunlight. *Environ. Sci. Technol.* **50**, 5017–5023 (2016).

Acknowledgments: We thank D. Aubin for contribution to the house dust samples collection. **Funding:** This research was supported by the National Sciences and Engineering Research Council (NSERC) Discovery Grant (RGPIN-2018-06), the Alfred P. Sloan Foundation Chemistry of the Indoor Environment Program (G-2019-11404), and New Frontiers in Research Fund (NFRFE-2019-00901). We acknowledge the support of instrumentation grants from the Canada Foundation for Innovation, the Ontario Research Fund, and the NSERC Research Tools and Instrument Grant. **Author contributions:** H.P. and D.Y. designed research. D.Y., Q.L., S.W., M.B., J.L., and H.K. performed research. Q.L. and J.P.D.A. contributed to indoor chemistry. D.Y., P.N., and D.S. contributed to organic synthesis. H.P., D.Y., Q.L., J.P.D.A., and D.S. analyzed data. B.O. contributed to sample collection. P.B. contributed to reporter cell measurement. H.P., D.Y., Q.L., and J.P.D.A. wrote the paper. **Competing interests:** The authors declare that they have no competing interests. **Data and materials availability:** All data needed to evaluate the conclusions in the paper are present in the paper and/or the Supplementary Materials.

Submitted 3 May 2022
Accepted 19 October 2022
Published 2 December 2022
10.1126/sciadv.abq7023

ScienceAdvances

Widespread formation of toxic nitrated bisphenols indoors by heterogeneous reactions with HONO

Diwen Yang, Qifan Liu, Sizhi Wang, Matin Bozorg, Jiabao Liu, Pranav Nair, Patrick Balaguer, Datong Song, Henry Krause, Boualem Ouazia, Jonathan P. D. Abbatt, and Hui Peng

Sci. Adv. **8** (48), eabq7023. DOI: 10.1126/sciadv.abq7023

Science Advances (ISSN 2375-2548) is published by the American Association for the Advancement of Science. 1200 New York Avenue NW, Washington, DC 20005. The title *Science Advances* is a registered trademark of AAAS.